Computational Particle Mechanics
https://doi.org/10.1007/s40571-025-00907-2

Developing a multi-scale model for the simulation of adsorption phenomena based on MD and CA: a Li-ion battery case study

Omid Ziaee[1,2] · Naeem Zolfaghari[1] · Mostafa Baghani[1] · Mahdi Bodaghi[3] · Majid Baniassadi[1]

Received: 11 October 2024 / Revised: 31 December 2024 / Accepted: 17 January 2025
© The Author(s) 2025

Abstract
Adsorption, an essential surface phenomenon, is involved in many industries, from water purification to energy storage and carbon capture, aiming at negative emission technologies. The need to synthesize new materials for these applications necessitates the development of new, flexible modeling tools to simulate complex conditions. This work introduces a multi-scale model to simulate various adsorption scenarios. It involves simulating the details of interatomic interactions in molecular dynamics simulations and scaling up to a laboratory scale through cellular automaton modeling. To showcase its capabilities, we utilized the simplest form of the model to simulate Li-ion adsorption on the surface of an anatase TiO_2 sheet. The probability of adsorption and desorption for a Li-ion is quantitatively determined through molecular dynamics simulations and subsequently incorporated into the cellular automaton model. This secondary model simulates the kinetic process of adsorption and quantifies the equilibrium degree of surface coverage across varying concentrations, facilitating comparison with the Langmuir isotherm. An inverse relationship between surface coverage and temperature is consistent with theoretical predictions. Given the model's computational efficiency, which complements molecular dynamics simulations, it offers extensive potential for extension across a broad spectrum of applications where adsorption, intercalation, diffusion, and other critical surface phenomena are fundamental.

Keywords Molecular dynamics · Cellular automaton · Adsorption · Lithium-ion battery

1 Introduction

Adsorption properties of materials have become a hotbed of research due to their surprisingly diverse applications across industries. From the food industry, where porous silica gels in packaging cling to moisture and keep contents fresh [1, 2], to coating technologies that rely on adsorption for strong adhesion [3], the reach of this phenomenon is vast. Biomedicine is used to deliver drugs directly to targeted cells and to assess the biocompatibility of implants [4, 5]. Environmental science applied to water treatment, air purification, carbon capture, and catalysis leverage adsorption power [6, 7]. Scientists even use it to study a material's surface intimately, revealing its chemical makeup, pore structure, and specific surface area [8].

However, perhaps the most exciting frontier application is for batteries. Researchers envision electrodes that adsorb charge-carrying ions onto their surfaces, dramatically improving charging speed, capacity, and lifespan, all by bypassing the traditional bulk absorption method [9–16]. This captivating field demands equally sophisticated simulation techniques. We need models that capture the intricate molecular-level interactions and the broader phenomena on the surface and can truly understand and harness the full potential of adsorption.

According to the International Union of Pure and Applied Chemistry (IUPAC), adsorption is "*An increase in the concentration of a dissolved substance at the interface of a condensed and a liquid phase due to the operation of surface forces. Adsorption can also occur at the interface of a*

✉ Mahdi Bodaghi
mahdi.bodaghi@ntu.ac.uk

✉ Majid Baniassadi
m.baniassadi@ut.ac.ir

[1] Department of Mechanical Engineering, University of Tehran, Tehran, Iran

[2] Department of Materials Science and Engineering, Boston University, Boston, MA, USA

[3] Department of Engineering, School of Science and Technology, Nottingham Trent University, Nottingham NG11 8NS, UK

Published online: 03 February 2025

condensed and a gaseous phase" [17]. Adsorption, a mesmerizing dance at the molecular scale, is orchestrated by the delicate interplay of interatomic forces. These microscopic magnets, acting as "surface forces," pull and hold adsorbate particles onto the adsorbent's surface, creating a concentrated layer. Unlike absorption, where the guest infiltrates the host's bulk, adsorption is a surface-exclusive phenomenon, a tango between sticking (adsorption) and unsticking (desorption). We gain insights into the particle's embrace and graceful release by analyzing these surface forces.

Modeling adsorption takes two distinct paths; the first is to dive deep, tracking individual particles and their interactions. Statistical tools such as averages and mean squares unlock the microscopic ballet, revealing the intricate forces at play. This approach is ideal for understanding fundamental mechanisms. Simulation methods such as molecular dynamics [18–20], Monte Carlo [21], diffusive particle dynamics [22], discrete element method [23], and cellular automaton [24, 25] lie in this category.

But what about larger scales, like laboratory experiments? Here, the second approach shines. We zoom out, assuming the adsorbent and particles form a seamless whole. This sacrifices detail for the ability to model over extended timescales, mimicking real-world observations.

Adsorption isotherms represent the graphical depiction of the equilibrium correlation between the quantity of adsorbate molecules adsorbed onto an adsorbent surface and the concentration or pressure of the adsorbate within the bulk phase at a constant temperature. Consequently, these isotherms fall under the category of second-type models. Of the most straightforward among these isotherms is the one proposed by Langmuir. This isotherm is called favorable adsorption isotherm (type 1), and the Langmuir equation most commonly characterizes it. Langmuir equation assumptions are:

1. Adsorbent is a gridded surface with energetically homogeneous adsorption sites with equal surface energy levels.
2. Adsorption is monolayer and local, meaning that once an adsorbate occupies an adsorption site, it cannot accommodate another particle, and they are fixed in their place.
3. Adsorbed particles do not interact with each other [26].

Langmuir equation determines the surface coverage of the adsorbent (θ) as a function of relative concentration (p) where k_{L} is the Langmuir constant, and it is related to adsorption capacity [26].

$$\theta = \frac{k_{\mathrm{L}} p}{1 + k_{\mathrm{L}} p} \tag{1}$$

Ultimately, the choice of the model boils down to our focus. Do we crave the intimate secrets of individual molecules or the grand choreography across time? Both approaches, like complementary lenses, offer unique perspectives on this fascinating surface phenomenon.

Particle-scale simulation methods such as DFT, MD, and MC hold immense power. Armed with first principles, interparticle interactions, and statistical sampling, they can accurately predict adsorption behavior. These methods have yielded fascinating results in adsorption research [27, 28]. However, their computational cost is immense, limiting them to situations with relatively small particle numbers and short timescales, far from the realm of typical applications. This dilemma creates a significant gap between the temporal and spatial scales accessible to experiments compared to simulations.

Continuum-based approaches, exemplified by Langmuir isotherms, offer a trade-off. They sacrifice some fine-grained details for the ability to model more extensive systems and make them computationally efficient and suitable for capturing larger-scale phenomena. However, the loss of detail can limit their precision, especially when intricate specifics become crucial for design purposes.

This fact highlights the complementary strengths and weaknesses of each approach. Particle-scale methods reveal the intricate behavior of individual molecules, providing invaluable insights into fundamental mechanisms. Continuum models, on the other hand, enable us to scrutinize through time, mirroring real-world observations and paving the way for practical applications. Ultimately, the choice hinges on the research question and the desired level of detail. Whether delving into the microscopic intricacies or observing the grand choreography, both approaches ultimately contribute to our understanding of this mesmerizing surface phenomenon.

For example, the inherent disparity between adsorption and desorption timescales poses a significant challenge for molecular dynamics (MD) simulations. While MD readily handles diverse adsorption processes, its converse, desorption, remains a formidable obstacle. As [29] demonstrates, desorption rates generally lag behind adsorption rates, leading to fewer observable desorption events within a typical MD simulation timeframe. Desorption, typically occurring at slower rates than adsorption under conventional temperatures, often necessitates post-processing techniques to extract relevant parameters after simulation completion and can compromise accuracy.

Hannah Fox's insightful research exemplifies this challenge on water adsorption onto MgO surfaces utilizing established interatomic potentials [30, 31]. Verifiable findings indicated a near-unity probability of adsorption (P_{Ads}) for adsorbates at equilibrium distance and low surface coverage [30]. However, determining the desorption probability (P_{Des}) proved problematic. Adsorbed particles remained

bound for hours in real time, exceeding the simulation duration. Fox et al. did not observe a desorption event within their simulated few seconds.

Consequently, a brute-force approach to simulating desorption would demand significantly extended simulations, rendered impractical by the inherent computational cost of MD. To address this, [30] implemented a formulation translating the system's interatomic potential to desorption rates, enabling reliable predictions at varying temperatures. However, these computations yielded single-particle insights, while the overall behavior, such as surface coverage, is often of primary interest. Therefore, a model remains necessary to translate these rates into isotherms for studying material adsorption at the macroscale.

We now introduce a multi-scale method that aims to bridge the chasm between the two classes mentioned above, leveraging the strengths of both MD and CA. This approach capitalizes on the formulation proposed by [30], enabling us to derive the parameters of a CA model directly from MD simulations.

Cellular automata (CA) represent an idealized physical system where time, space, and physical attributes are restricted to discrete sets. This approach creates a discrete model that evolves based on a pre-defined set of rules. Von Neumann's pioneering work in the late 1940s laid the foundation for this powerful approach, which has since found applications across diverse scientific domains [32–34].

A cellular automaton (CA) is a discrete dynamical system that evolves based on simple, local interaction rules. It consists of the following key components:

- Lattice/Cells: The CA is defined on a grid (or lattice) composed of discrete units called cells. Depending on the application, the grid can be one-dimensional, two-dimensional, or higher-dimensional.
- Cell States: Each cell in the lattice has a finite set of possible states. For instance, states can be binary (e.g., 0 or 1) or more complex (e.g., a range of integers or colors).
- Neighborhood: The neighborhood of a cell consists of the set of adjacent cells that influence its state. In one-dimensional CA, neighborhoods typically include the cell and its immediate neighbors (e.g., the cells on the left and right). In two-dimensional CA, neighborhoods might consist of the four nearest cells (von Neumann neighborhood) or eight surrounding cells (Moore neighborhood).
- Transition Rules: A set of deterministic or probabilistic rules governs how the state of each cell changes at each time step. These rules define how a cell's current state and neighbors determine its next state.
- Time Steps: The evolution of the CA occurs in discrete time steps. At each step, all cells update their states simultaneously based on the transition rules (synchronous updates).
- Initial Configuration: The CA starts from an initial configuration, which defines the state of every cell at time $t = 0$. The initial setup can be pre-defined, random, or determined by specific constraints.
- Boundary Conditions: These specify how the edges of the grid behave. Common boundary conditions include periodic (wrapping around the grid edges), fixed (static values at the edges), or reflective (mirroring the edge states).

A simple one-dimensional CA system is presented in Fig. 1. The state of the system at timestep t_n, the neighborhood and the local rules are given. For this system, we assumed periodic boundary conditions, so the cells at the boundaries are considered neighbors. Here, white represents the state 0, and black is 1. The transition rules determine the next state of the cell based on its own and it neighbors' state, so, for example, per rule 1, if a cell is zero, and both of its immediate neighbors are 1, this cell's state will change to 1 in the t_{n+1} timestep, and per rule 2, if any cell at state 0 has a neighbor with state one on the left and zero on the right, it will remain zero for the next timestep. The state of the system at the timestep t_{n+1}, the rule that was applied to each cell is shown at the bottom of Fig. 1.

The system's state at timestep t_n, the neighborhood and the local rules are provided. This system assumes periodic boundary conditions, meaning the cells at the boundaries are treated as neighbors. The state of the system at timestep t_{n+1}, the specific rule applied to each cell is shown at the bottom left of Fig. 1. Here, white represents state 0, and black represents state 1.

The transition rules determine the next state of each cell based on its current state and the states of its immediate neighbors. For instance:

- Rule 1: If a cell is in state zero and both of its immediate neighbors are in state 1, the cell's state will change to 1 in the next timestep (t_{n+1}).
- Rule 2: If a cell is in state zero and has a neighbor with state 1 on the left and 0 on the right, it will remain in state zero at t_{n+1}.

The allure of CA lies in its ability to provide simple yet effective models for complex systems. Researchers elegantly demonstrated how the collective behavior of a system could arise from the summation of individual, often simple, components [35]. This fact highlights a key feature: Even when the microscopic properties are fully understood, global behavior can exhibit novel laws beyond the reach of individual interactions. The power of CA resides in the intuitive rules governing interactions between neighboring sites, allowing us to capture emergent phenomena not readily apparent from separate components.

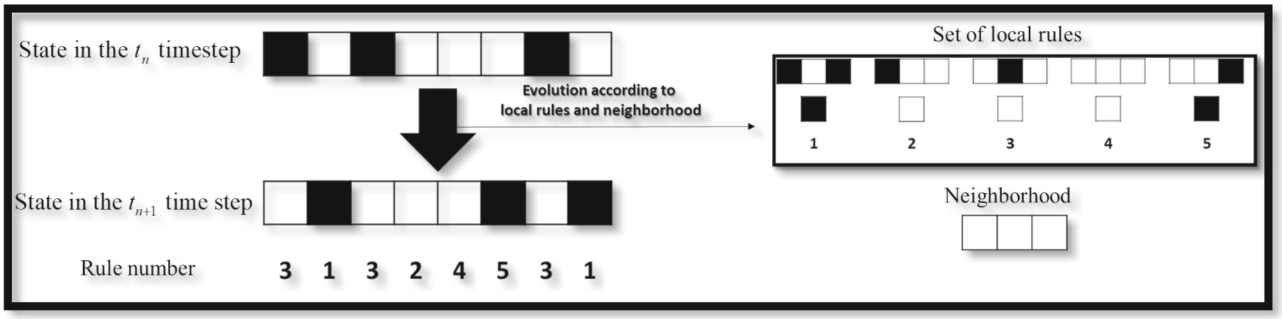

Fig. 1 A typical one-dimensional CA model

The inherent intuitiveness of CA models renders them highly adaptable, enabling simulations of Li-ion dynamics within battery electrodes, as demonstrated by [36, 37]. However, meticulous attention is necessary when defining the local rules, as [38] also highlights that factors such as movement scenarios and adsorbent shapes can significantly influence model behavior.

This work presents a multi-scale model for adsorption phenomena, elucidated through an example focusing on the prevalent Type 1 (favorable) adsorption isotherm, typically characterized by the Langmuir equation. We propose a complementary model that seamlessly integrates CA and MD, encompassing particle-scale intricacies and yielding outputs familiar to laboratory scientists. We leverage the work of Fox [30, 31] to convert MD simulation results into desorption probabilities, subsequently utilized within the probabilistic cellular automaton (CA) model.

In Sect. 2, we discuss the details of the CA and MD models, and how we aim to interpret the MD model's results to get the CA model parameters. In Sect. 3, we first show the MD simulations for two temperatures and how we calculated the adsorption and desorption probabilities for the CA model. This is followed by the CA model results and the two adsorption isotherms for 300 and 750 K. A comparison of our model results with a similar experiment is presented at the end of this section. Finally, in Sect. 4, we highlight the key findings and potential of the existing model and propose further developments for this protocol.

2 Method

2.1 CA implementation for the intended adsorption scenario

This research leverages a cellular automata (CA) model inspired by the work of [36]. To simplify the analysis, we implement assumptions consistent with the Langmuir isotherm. It is important to note that these assumptions readily adapt to more complex scenarios, thereby ensuring the model's broad applicability.

Typically, the setup of a CA model involves two crucial steps: initial configuration and time evolution. The initial configuration entails particle distribution, force specification, and definition of boundary conditions (local rules).

Consider a box filled with non-interacting particles free moving in a 3D space (Fig. 2). Since we are only interested in the adsorption behavior, not the behavior of these moving particles, the simplest possible model is considered for their dynamics. This assumption can be easily modified by the use of more complicated dynamics such as dissipative particle dynamics [22], Langevin equations [39], or Monte Carlo moves based on a more complicated interaction potential [21, 28]. Therefore, in our simple mode, particles do not feel each other and may even occupy the same position in some simulation instances.

Each side of the box treats these particles differently. The four lateral sides act as periodic boundaries, which means that when a particle exits the box through one side, it re-enters from the opposing side at the same position and with unchanged velocity. This approach effectively simulates an infinite system by eliminating edge effects and ensuring a continuous environment for particle movement, as previously demonstrated [40]. On the other hand, the top wall reverses the z-component of the velocity of impacting particles and acts as a rebounding surface. Finally, the bottom box is where the adsorbent resides. Each particle colliding with this surface has a chance of being adsorbed or rebounded based on the adsorption probability.

It is noted that the box is cellular, meaning that the particles are only allowed to occupy positions that are integer multiples of the lattice constant (1 unit was assumed throughout our simulations). Each cell state transitions between 0 and 1 during each time step, signifying either an unoccupied or occupied cell. This simplified model does not require the integration of any equations, and the particles move in 3D based on the probability of movement (random walk-like movement). This behavior can be compared to diffusion-limited

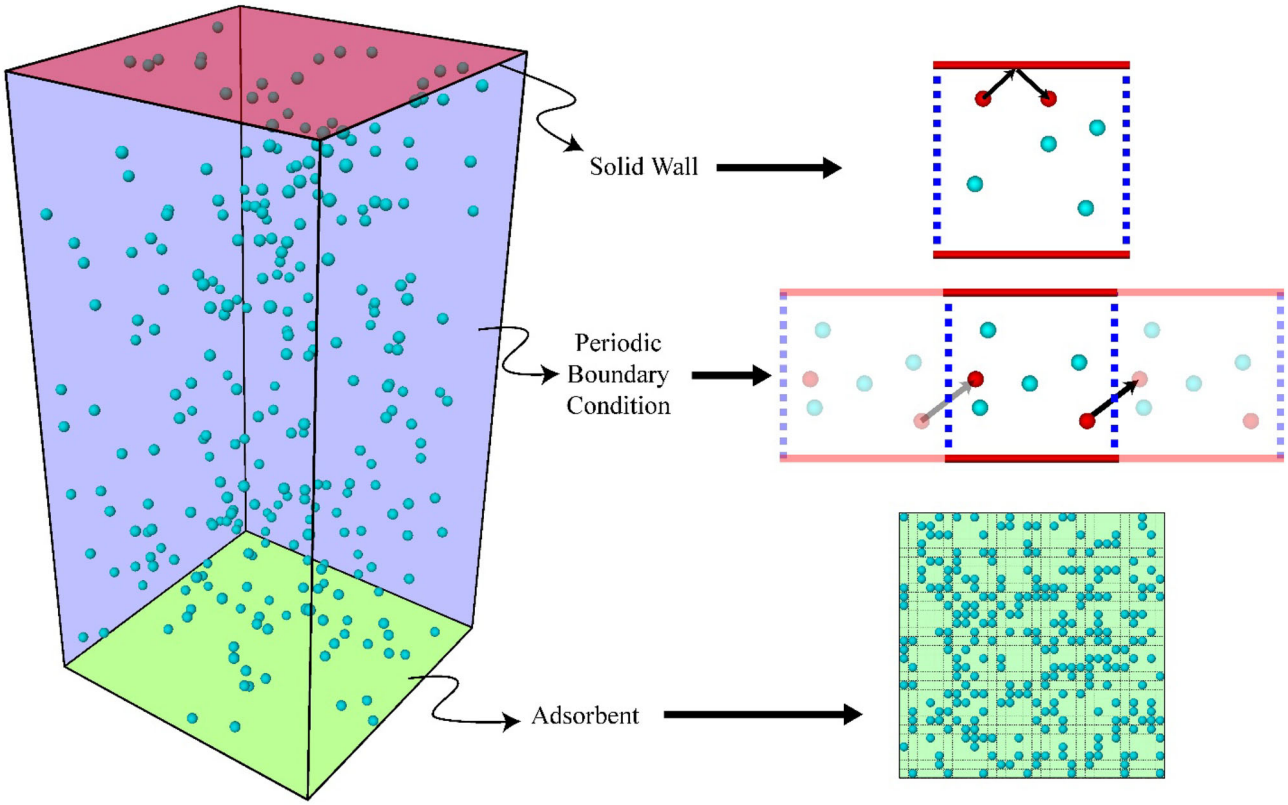

Fig. 2 Simulation box. The box's lateral walls have periodic boundary conditions, and the box is re-entered from the opposing wall whenever a particle passes through it. The top surface reverses the perpendicular velocity of the impacting particles, acting as a rebounding wall. The bottom surface is the adsorbent layer

aggregation in that the particles randomly diffuse until they collide with the adsorbent, where it is decided whether they are adsorbed [41].

Before the simulation's commencement, several particles proportional to their concentration are randomly dispersed throughout the box. We assume that these particles are in the gas phase, necessitating the use of the Maxwell–Boltzmann distribution to assign their velocities. Consequently, their velocity magnitudes follow a normal distribution, as outlined by [42]. The movement of each particle directly correlates with its assigned velocity, reflected in the probability of movement during each time step. The system's temperature is constant throughout the simulation, ensuring that movement probabilities remain unaltered.

Three random numbers are generated for each particle to implement the particle movement, representing their respective movement probabilities in each spatial dimension. The sign of each random number dictates the direction of movement, while its magnitude signifies both the movement probability and the intended velocity. For particles not subject to interacting forces, isotropic movement is desired. In other words, the probability of movement to any neighboring cell should be equal. As demonstrated in the previous work by [38], this can be achieved by implementing equalizer coefficients.

The model presents a nuanced challenge requiring careful consideration. In some scenarios, significant particle adsorption onto the surface can occur. This phenomenon can alter the properties of the remaining free-moving particles. For instance, if a substantial portion of the adsorbate becomes immobilized, the remaining free particles typically exhibit diminished movement probabilities along the Z-axis. Consequently, two key characteristics of the moving particle population are altered: concentration and velocity. This phenomenon is effectively equivalent to a reduction in the system's apparent temperature.

Two potential strategies can be employed to address these situations. The first involves adding new particles to the simulation box, replenishing the free-moving population and mitigating adsorption effects. Alternatively, the movement probabilities of the remaining free-moving particles could be reset, effectively re-establishing their initial kinetic state (temperature).

With initial conditions established, the automaton is poised for evolution according to its local rules. As mentioned, each particle is assigned three probabilities, inherently correlated with the Maxwell–Boltzmann distribution. Collisions between free-moving particles are deemed negligible in their impact on the system's equilibrium behavior and are, therefore, disregarded.

As the automaton evolves, particles colliding with the box's sides are treated according to the defined boundary conditions. For particles impacting the top surface, their velocity sign in the z-direction is reversed while the magnitude remains conserved. Particles reaching planes perpendicular to the X and Y axes re-enter the box on the opposite side.

Adsorption occurs solely on the bottom surface. The adsorbent is modeled as a heterogeneous flat surface, permitting only local monolayer adsorption. Interaction is limited to the attractive force between particles and the adsorbent, excluding any interaction between adsorbed particles themselves. During each time step, a particle placed on the adsorbent surface may adhere (adsorb) based on a predetermined probability. Conversely, previously adsorbed particles may desorb according to a separate probability. These probabilities of absorption and desorption are denoted by P_{ads} and P_{des}, respectively.

Our analysis has established a connection between the model parameters P_{Ads} and P_{Des} and the k_{L} coefficient of Langmuir's isotherm (Eq. 2). This relationship is expressed as follows:

$$k_{\text{L}} = 0.1342 \frac{P_{\text{Ads}}}{P_{\text{Des}}} \tag{2}$$

When the non-homogenous movement rule is used, we have shown that the prefactor magnitude is equal to the average probability of movement in each principal direction. When we use the movement rule that yields homogenous speed in three dimensions, the prefactor should be changed to 0.1957 as Eq. (2) is for when the non-homogenous movement rule is used. In our previous work, we have shown why the average probability of movement in each timestep for each direction is equal to 0.1342. For both negative and positive directions, it would be 0.2684 [38]. We defined the homogenous speed movement rule because the particle would move based on the magnitude of its velocity vector. Therefore, the probability of movement in each direction is:

$$\text{Movement probability} = \frac{(1 - 0.2684)^3}{2} = 0.1957 \tag{3}$$

The equation to correlate model parameters with k_L is:

$$k_{\text{L}} = 0.1957 \frac{P_{\text{Ads}}}{P_{\text{Des}}} \tag{4}$$

In summary, our CA model has only three parameters requiring calibration: temperature, P_{Ads}, and P_{Des}. Temperature directly influences the movement probabilities of the free-moving particles within the system. The other two parameters determine the interaction between the adsorbent surface and the moving particles. We can generate adsorption isotherms by systematically adjusting these three parameters and monitoring the resulting number of adsorbed particles. The beauty of this CA model lies in its simplicity. With minimal parameters, it captures the essential dynamics of the adsorption process, enabling the generation of readily interpretable isotherms even for complex, large-scale systems.

The desorption probability can be calculated using various methods. We propose using MD and a simple formulation proposed by [31] to calculate this coefficient. Consider a system of molecules where a portion is adsorbed onto an adsorbent surface while others desorb from it. We denote the adsorbate density at any location. $r_{j,k}$ as $\rho\left(r_{j,k}\right)$. Normalizing this quantity yields the spatial distribution of adsorbates, represented by $\overline{\rho}(z)$. Consequently, $\overline{\rho}(z)\mathrm{d}a\mathrm{d}z$ signifies the probability of encountering an adsorbate particle within a volume element $\mathrm{d}a\mathrm{d}z$. Through meticulous calculations, [30, 31] demonstrated that the desorption rate per unit time per adsorbed molecule can be determined via the following equation:

$$\gamma = \frac{\sqrt{k_{\text{B}} T / 2\pi m}}{\int_{-\infty}^{z0} y(z)\mathrm{d}z} \tag{5}$$

where k_B, T, and m are Boltzmann constant, temperature, and the mass of adsorbates, respectively. In addition, $y(z)$ is

$$y(z) = \frac{\overline{\rho}(z)}{\rho_0} \tag{6}$$

with ρ_0 being the mean density of molecules in the gas phase. It is assumed that this probability distribution function can be expressed in terms of the potential of mean force by [31, 43]:

$$y(z) = \exp\left(-\frac{\phi(z)}{k_{\text{B}} T}\right) \tag{7}$$

The potential of mean force (PMF) for a surface with a normal in z-direction with the assumption of ergodicity of the system is:

$$\phi(z) = -\int_{\infty}^{z} \langle F_z \rangle_z \, \mathrm{d}\hat{z} \tag{8}$$

The force acting on adsorbate particles (F_z) can be calculated using MD simulations. Then, using Eqs. (5, 7, and 8) in reverse order results in the desorption rate used in the CA model.

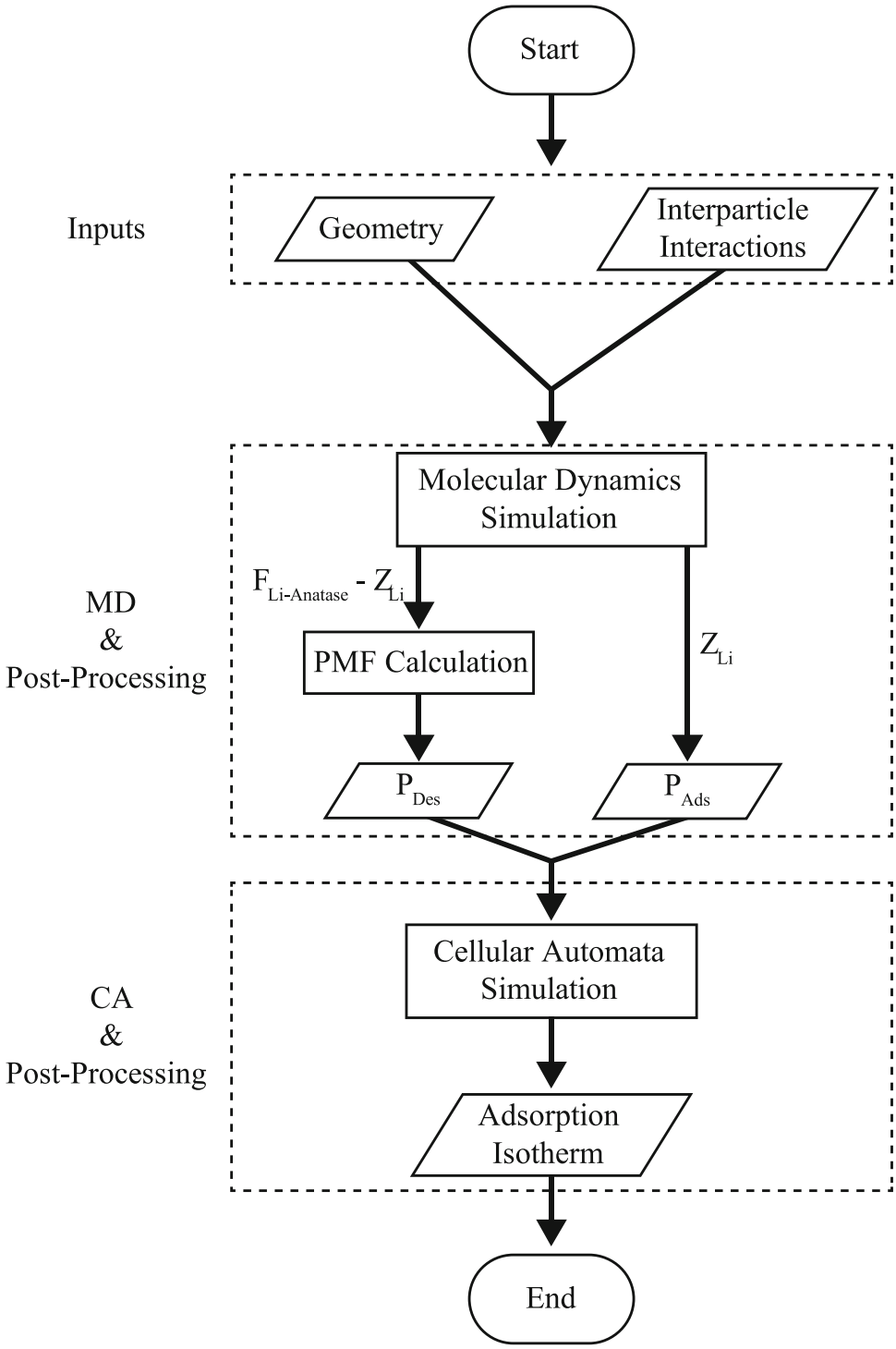

Fig. 3 Algorithm of MD-CA method for the simulation of adsorption

3 Summary of the method

To summarize our method, Fig. 3 schematically outlines the pseudo-algorithm required to carry out this approach, divided into two main stages: Molecular Dynamics Simulation and Cellular Automata Simulation. The steps are as follows:

1. Molecular dynamics simulation
   - Preparation: This step involves setting up the simulation environment by defining the geometry of the adsorbent system and specifying the interparticle interactions between the adsorbent and adsorbates.

- Simulation: In this phase, particles (adsorbates) are "shot" toward the adsorbent surface, and their interactions with the adsorbent layer are tracked. Key outputs include the interaction forces between the adsorbent and the adsorbates, as well as the relative positions of adsorbates concerning the adsorbent.
- Post-Processing: Using the simulation data, the probabilities of adsorption (P_{Ads}) and desorption (P_{Des}) are calculated. These values are obtained by converting the raw simulation outputs into meaningful physical quantities using appropriate unit conversions.

2. Cellular automata simulation

- Preparation: This involves setting up the geometry of the simulation grid and defining the local rules that govern particle dynamics.
- Simulation: The adsorption–desorption dynamics of particles are simulated using the coefficients calculated from the Molecular Dynamics stage (P_{Ads}) and (P_{Des}).
- Post-Processing: The simulation results are analyzed to compute macroscopic outputs, such as adsorption isotherms, diffusivity, and other relevant properties of the system.

4 Results and discussion: adsorption of Li-ions on anatase sheet

As mentioned before, utilizing the absorption of charge carriers onto the battery electrodes during the charge/discharge cycles is promised to improve battery performance [44]. Thus, as a case study, we investigate Li-ions' adsorption onto the anatase polymorph of TiO_2. Anatase is among other metal oxides being investigated, which can deliver stable and high specific capacity, unlike conventional graphitic electrodes [44–46].

To generate the geometrical configuration of the sheet, we iteratively replicated the unit cell of anatase (Fig. 4) in 3D until the desired dimensions were achieved. For this specific example, a sheet with dimensions of 49.1 Å × 49.1 Å × 28.1 Å was generated.

We employed LAMMPS for all molecular dynamics (MD) simulations. A time step of 1 fs was chosen, in conjunction with the Berendsen barostat [47] and Nose–Hoover thermostat [48] to regulate pressure and temperature, respectively.

Interparticle interactions in this system are governed by Buckingham's potential for short-range repulsion, van der Waals attraction, and Coulomb's potential for electrostatic interactions. This combined potential is expressed as follows:

$$U\left(r_{ij}\right) = A_{ij}\exp\left(-\frac{r_{ij}}{\rho_{ij}}\right) - \frac{C_{ij}}{r_{ij}^{6}} + \frac{q_i q_j}{r_{ij}} \tag{9}$$

Table 1 Coefficients of Buckingham potential [49]

Interaction	$C_{ij}\left(\text{eV Å}^6\right)$	$\rho_{ij}\left(\text{Å}\right)$	$A_{ij}\,(\text{eV})$
Ti–O	12.59	0.194	16,957.710
Ti–Ti	5.25	0.154	31,120.528
O–O	30.22	0.234	11,782.884

r_{ij} is the distance between particles, and q_i and q_j are the partial charges of them. The Buckingham potential accounts for the repulsive and attractive forces arising from electron overlap at short distances. The repulsive term dominates at very close interparticle distances, preventing particle overlap. As the distance increases, the attractive term becomes dominant, leading to weak van der Waals forces. The Coulomb potential describes the electrostatic interaction between charged particles. The potential energy is positive and repulsive when like charges are brought close together and negative and attractive for opposite charges. Particle–particle particle-mesh (PPPM) solver accounts for long-range interactions with a cut-off radius of 10 Å.

The parameters in this function are optimized for TiO_2 [49], and we have tabulated them in Table 1. The partial charges are + 2.196, − 1.098, and 0.549 for Ti, O, and Li, respectively [50]

The initial stage of our simulation involves relaxing the anatase sheet at a temperature of 300 K. This process comprises two key steps:

1. Geometry Optimization: First, we optimize the sheet's geometry using an energy tolerance of 10^{-6}. This step ensures the initial configuration is free of potential energy minimization artifacts and overlapping particles.
2. Dynamic Relaxation: With the bottom-layer atoms fixed, we perform a dynamic relaxation using three different ensembles:
   - NPT: This ensemble allows the temperature and pressure to equilibrate at zero pressure and 300 K for 100 picoseconds (ps).
   - NVT (Canonical): We then switch to the NVT ensemble, fixing the temperature (300 K) for another 100 ps. This further refines the system's configuration at the target temperature, lifting the constraint on pressure.
   - NVE (Microcanonical): Finally, we employ the NVE ensemble for 100 ps, where both the temperature and pressure constraints are removed. This supposition ensures a stable and well-equilibrated starting point for the subsequent adsorption studies.

More details on equilibration for this can be found in the work of [51]. The final relaxed configuration of the sheet

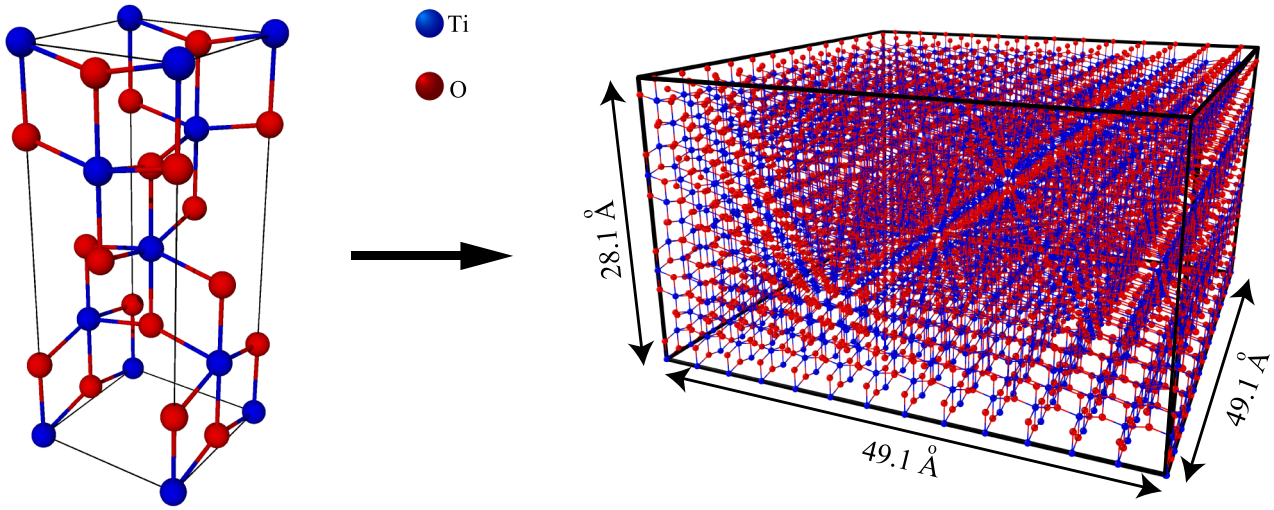

Fig. 4 Anatase unit cell and anatase sheet with dimensions 49.1 Å × 49.1 Å × 28.1 Å

serves as the foundation for our Li-ion adsorption\desorption investigation. We introduce Li-ions into the simulation box and monitor their interactions with the sheet. This method includes recording the interatomic forces between Li-ions and the anatase sheet and the position of each Li-ion throughout the simulation. These data are then used to calculate the desorption rate.

The investigation of adsorption probability involved the sequential addition of Li-ions to the simulation box utilizing the LAMMPS *create_atoms* command. These ions are located randomly within a rectangular box defined by the coordinates x, $y \in [5{,}40]$ $z \in [30, 35]$. This choice ensured the ion was positioned directly above the sheet and on the verge of electrostatic interaction (considering a cut-off distance of 12.5 Å). To comply with the Langmuir assumption of non-interacting adsorbed particles, ions were introduced one at a time. Each atom received a random velocity solely in the z-direction based on its temperature and was granted a 1.5 ps interaction period with the anatase sheet. Its z-coordinate was recorded throughout this time. After this period, the LAMMPS *delete_atoms* command was used to remove the ion from the simulation box, and another Li-ion substituted it at a random location. 100 Li-ions were bombarded onto the anatase sheet at each temperature. Figure 5 portrays the findings of this simulation conducted at 300 K and 750 K, alongside the corresponding histogram of the final z-coordinates of the Li-ions displayed on the right.

Figure 5 shows the z-coordinate of 100 Li-ions colliding with the anatase sheet. The cut-off distance for long-range r-6 interactions above the top of the anatase sheet is also shown in Fig. 5a with a dashed red line. All the ions are initially placed outside the long-range cut-off. From Fig. 5a, it is deduced that some ions rebound after the collision and then get adsorbed. These are deemed "not adsorbed" in the later calculations as the first impact has not yielded adsorption. The figures on the right-hand side (Fig. 5b, d) show the histogram of the z-coordinate of these ions 1.5 ps after being placed above the anatase sheet. Comparing Fig. 5a, c, it is observed that, on average, the ions impact the surface after a shorter time because of higher velocities. In addition, the rebounding ions may get further distances after impact. In addition, Fig. 5b, d shows that increasing temperature shifts the end z-coordinate further away from the sheet as the equilibrium distances increase at elevated temperatures. These results are used for the calculation of adsorption probability.

Table 2 Calculation of CA model parameters of adsorption and desorption probabilities (P_{Ads} and P_{Des}) from MD model results

T (K)	Desorption rate (s^{-1})	P_{Des}	P_{Ads}
300	4.35E + 10	0.0435	0.91
750	1.31E + 11	0.1312	0.94

Adsorption probability (P_{Ads}) is calculated by first measuring how far the Li-ion has rebounded after colliding with the anatase sheet. Considering a radius of 1.4 Å and 1.45 Å for Ti and Li atoms, respectively, those Li-ions that bounced back more than 3 Å after the initial impact are not absorbed. Considering this criterion, the adsorption probability is calculated by counting the number of the adsorbed Li-ions concerning the total number of the impacting Li-ions.

On the other hand, desorption probability requires more calculation based on the equations of the former section. To this end, force–distance curves of impacting ions are stored, and smooth spline fits are used to calculate the required integrals. Figure 6 showcases a force–distance curve at 300 K and the corresponding PMF. The PMF is calculated by plugging Fig. 6a into Eq. (8). The desorption probability is then

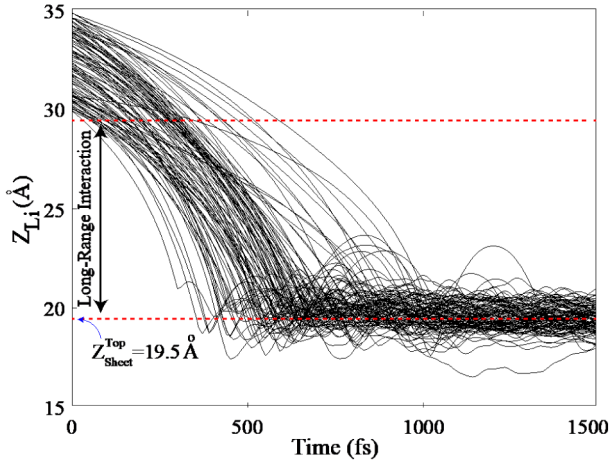

a) Time-History of Z-Coordinate of Li-Ions (T=300 K)

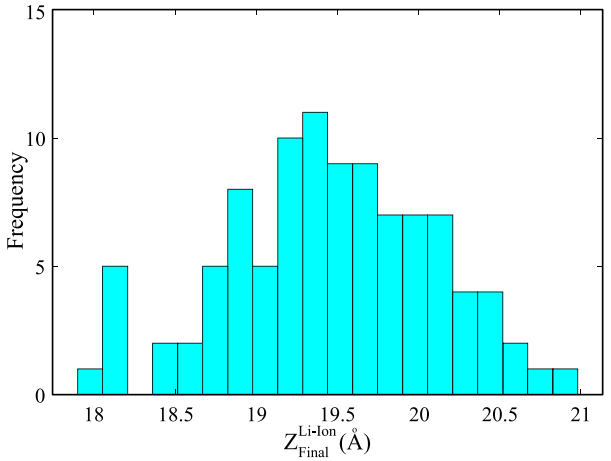

b) Histogram of Final Z-Coordinate of Li-Ions (T=300 K)

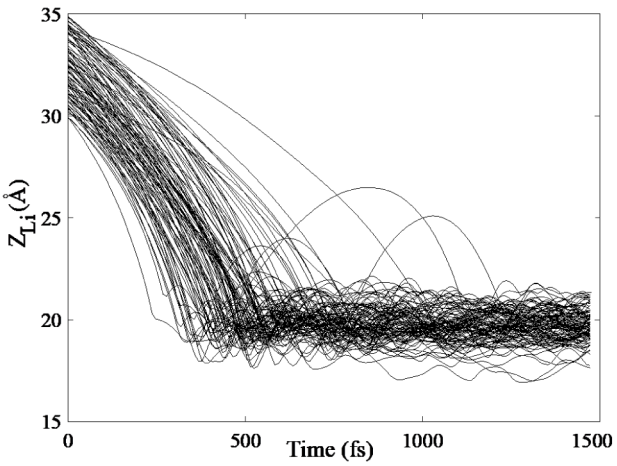

c) Time-History of Z-Coordinate of Li-Ions (T=750 K)

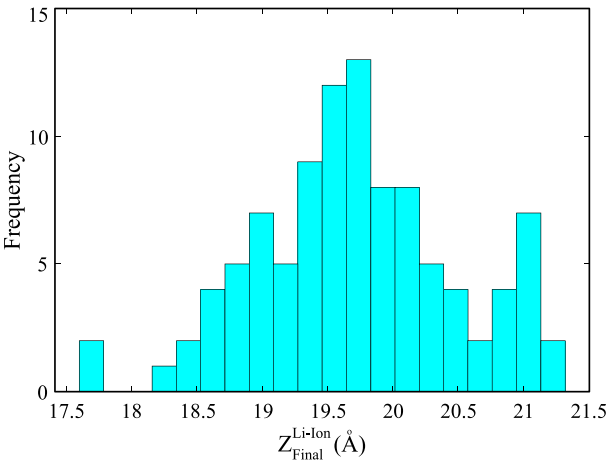

d) Histogram of Final Z-Coordinate of Li-Ions (T=750 K)

Fig. 5 Adsorption of Li-ions on the anatase sheet at T = 750 K. **a**, **c** *Z*-coordinate of individual Li-ions. **b**, **d** Histogram of *z*-coordinates after 1.5 ps

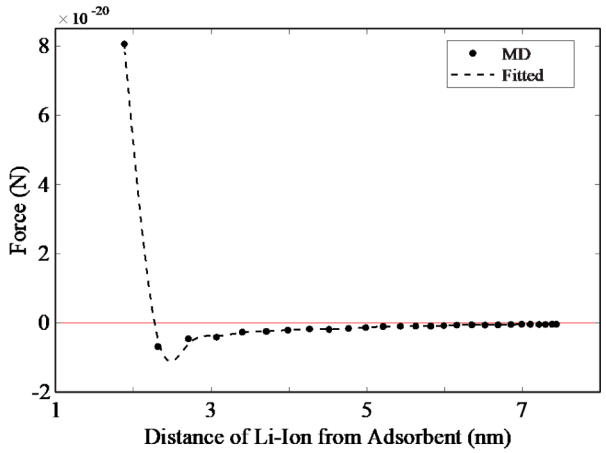

a) Force-Distance Curve

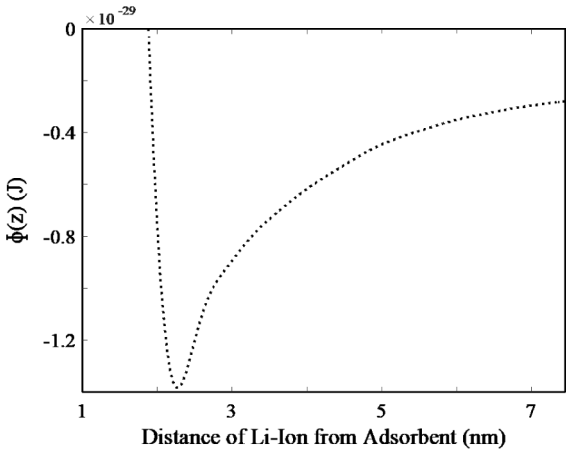

b) $\phi(z)$

Fig. 6 Calculation of potential of mean force for $T = 300$ K

Table 3 Extracted coefficients of Langmuir equation from the isotherms of Fig. 5

Temperature (K)	Fitted k_L (from CA model results)	k_L from Eq. (4) (theoretical value)	Error (%)	R-squared
300	3.9764	4.2214	6.1614	0.99967
750	1.3522	1.3570	0.3550	0.99971

The R-squared values and minor differences between the theoretical and CA model's k_L show close accordance with theoretical conditions

calculated by inputting the PMF (Fig. 6b) into Eq. (7) and then Eq. (5), which is presented in Table 2. In summary, the force exerted on the lithium-ion should be used sequentially to calculate the desorption rate from Eqs. (8, 7, and 5).

Conversion of units is required to translate the results of the MD simulations to be an input to the CA model. First, the particle velocity–temperature correlation should be set up. We assume that the free-moving Li-ions movement probability (velocity) and the cell size are considered to be the same for all temperatures, but the time step varies. This is done by equalizing the adsorbent cell size to the distance between two of anatase's octahedral sites since they are reported to be stable adsorption sites. The effect of thermal expansion is neglected in this case study. For example, for $T = 300$ K, the adsorbent cell size is measured to be 3.776 Å, i.e., the adsorbent's cell size. The movement probability for each direction is 0.1957 (Eq. 4), and each time step is 1 ps, while according to the Maxwell–Boltzmann distribution, the average velocity is 475 m/s. When temperature increases, the model's time step is reduced (less than 1 ps), while the movement probability in each time step stays the same, so the real-world speed would be increased. In this sense, if at 300 K each time step 1 ps, at 750 K, the average velocity is 750 m/s, and each CA timestep equals $\frac{475}{750} * 1\,\text{ps} = 0.63\,\text{ps}$. This calibration allows one to modify the CA's model size of the adsorbent and time step based on the available adsorption sites and temperature of the MD model.

Inputting these rates into the model as P_{ads} and P_{des}, the Langmuir isotherm is presented in Fig. 7

Table 3 presents the fitted k_L, R-squared (R^2) and the k_{L} calculated from Eq. (4). The k_{L} is calculated using the nonlinear least squares (NLLS) optimization method, which essentially minimizes the sum of the squared vertical distances (residuals) between the data points and the fitted curve. As can be seen, increasing the temperature reduces the surface coverage.

Since we can generate the adsorption isotherms from the CA model, we can use the isotherms to compare the model results with others. This study assumes Langmuir's assumptions for the adsorption of Li-ions onto a sheet of anatase and measures the equilibrium surface coverage of the pristine anatase sheet. Due to the lack of the previous works on this exact adsorption scenario, we can consider a case with conditions close to ours. [52] reported the Langmuir adsorption isotherm of Li-ions onto a specific TiO_2 precursor. Their adsorption experiment was done in a different environment with a slightly different adsorbent. Although the adsorbent material and adsorption conditions are not precisely the same, since they reported the R-squared of the Langmuir adsorption isotherm equation to their experimental results is 0.9942, we can use their result to make a comparison. We can do so by comparing our and their maximum degree of coverage. Calculating the experimental maximum degree of coverage can be done by dividing the maximum surface coverage attained, to the maximum theoretical limit derived from Langmuir's equation.

Table 4 Comparison of the proposed simulation model with an adsorption experiment

Method	Adsorption condition	Temperature (K)	Maximum degree of coverage
MD-CA simulation	Li-ion onto anatase sheet	300	0.808
Experiment [52]	Li-ion onto TiO_2 precursor	298	0.869

Table 4 summarizes our model results and the experiment in [52]. The results show an error of 7%, which is quite acceptable for a theory-driven model and demonstrates its ability to simulate similar scenarios. One point to consider is that our CA model uses results calibrated for 298 K, whereas the experiment in [52] was conducted at 300 K. The study in [52] demonstrated a strong direct relationship between adsorption capacity and temperature between 298-313K, which could contribute to the observed difference in our results.

5 Conclusion

We developed a multi-scale method for the modeling of adsorption. The model begins with calculations of adsorption and desorption features using molecular dynamics and tunes the local rules of a cellular automata model to analyze the behavior of adsorbate on the adsorbent. Depending on the

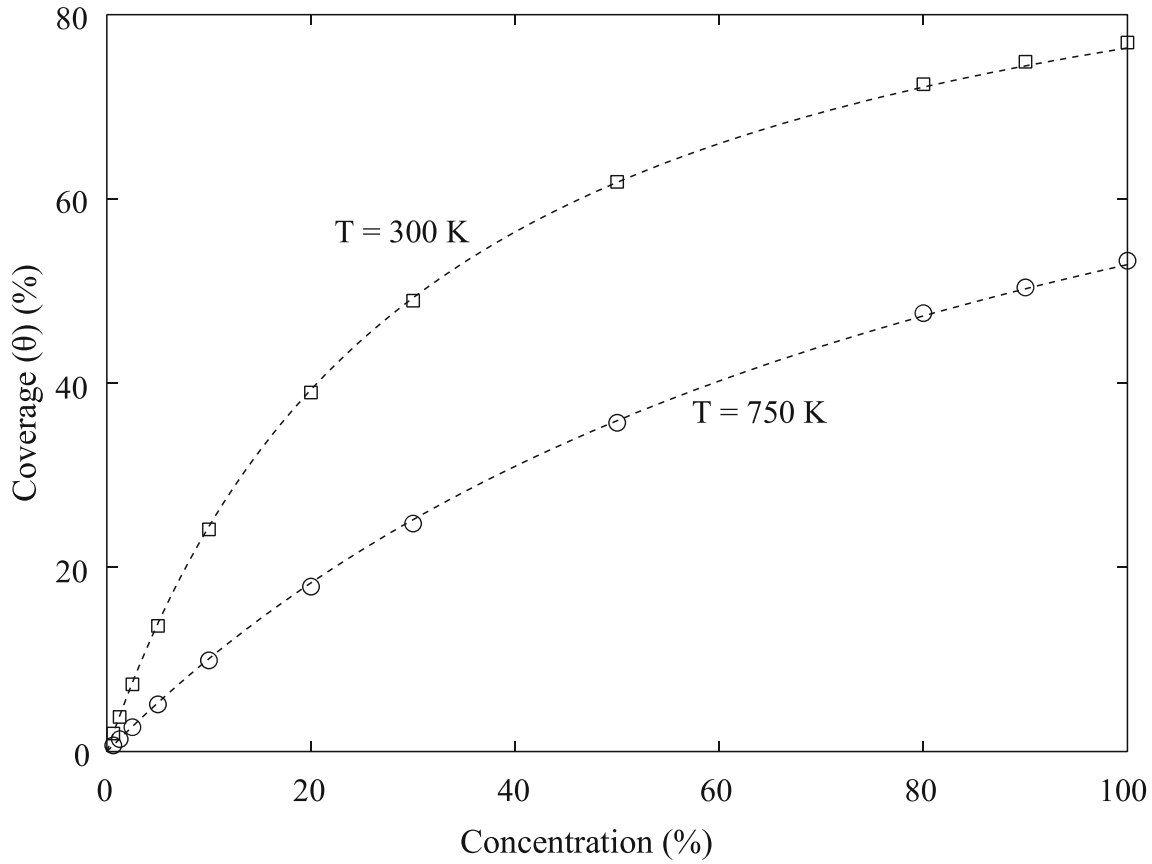

Fig. 7 Isotherms for adsorption of Li-ions on the surface of anatase sheet at 300 K (squares) and 750 K (circles)

local rules assumed, the model's output can be adsorption isotherms or any other parameter associated with adsorption. The absorption of Li-ions on the surface of the anatase sheet was studied, and isotherms at two temperatures were reported. The closeness of the maximum degree of coverage for our cases underlines the model's ability to effectively simulate Li-ions absorption onto an adsorbent, as long as the CA model's parameters are meticulously derived from appropriate experiments such as an MD simulation. In this work and previous work, we have shown that this model can simulate theory-driven adsorption isotherms with very high accuracies [36–38]. While the comparison with a similar experiment yielded comparable results, further development of this model is necessary to extend its applicability to other experiments. These traits must be theoretically predicted or experimentally measured and incorporated as CA parameters to account for surface imperfections or other adsorbent characteristics. This model explicitly assumes the adsorbate is in the gas phase with no interactions. Therefore, when the behavior of the adsorbate in a solvent plays a crucial role, the model must be adjusted to account for the interactions of free-moving adsorbates and formulated accordingly.

The current example model is the simplest one and can be easily modified to capture diffusion in the bulk of the adsorbent, intercalation within the matter, creation of solid–electrolyte interface (SEI), sputtering, and many other surface phenomena, as previously shown [36–38]. In addition, the dynamics of the free-moving particles can be modified using more complicated models such as diffusive particle dynamics, off-lattice models, and molecular dynamics. The model's simplicity lies in the substitution of the adsorbent by simple local rules, which neglects the details of its mechano-chemistry.

Author contributions Omid Ziaee helped in data curation (lead), formal analysis (supporting), methodology (equal), software (lead), validation (equal), visualization (supporting), writing/original draft preparation (equal), and writing/review and editing (equal). Naeem Zolfaghari helped in conceptualization (equal), data curation (supporting), formal analysis (lead), methodology (lead), software (equal), visualization (lead), writing/original draft preparation (equal), and writing/review and editing (equal). Mostafa Baghani helped in conceptualization (equal), project administration (equal), resources (equal), supervision (equal), validation (equal), and writing/review and editing (equal). Mahdi Bodaghi helped in conceptualization (equal), methodology (equal), project administration (equal), resources (equal), software (equal), supervision (equal), validation (equal), and writing/review and editing (equal). Majid Baniassadi helped in conceptualization (equal), methodology (equal), project administration (equal), resources (equal), software (equal), supervision (equal), validation (equal), and writing/review and editing (equal).

Data availability The data supporting this study's findings are available from the corresponding author upon reasonable request.

Declarations

Conflict of interest The authors have no conflicts to disclose.

Open Access This article is licensed under a Creative Commons Attribution 4.0 International License, which permits use, sharing, adaptation, distribution and reproduction in any medium or format, as long as you give appropriate credit to the original author(s) and the source, provide a link to the Creative Commons licence, and indicate if changes were made. The images or other third party material in this article are included in the article's Creative Commons licence, unless indicated otherwise in a credit line to the material. If material is not included in the article's Creative Commons licence and your intended use is not permitted by statutory regulation or exceeds the permitted use, you will need to obtain permission directly from the copyright holder. To view a copy of this licence, visit http://creativecommons.org/licenses/by/4.0/.

References

1. Gaikwad KK, Singh S, Lee YS (2018) High Adsorption of ethylene by alkali-treated halloysite nanotubes for food-packaging applications. Environ Chem Lett 16:1055–1062. https://doi.org/10.1007/s10311-018-0718-7
2. Lee Y-C, Weng L-C, Tseng P-C, Wang C-C (2015) Effect of pressure on the moisture adsorption of silica gel and zeolite 13X adsorbents. Heat Mass Transf 51:441–447. https://doi.org/10.1007/s00231-014-1442-x
3. Silva-Bermudez P, Rodil SE (2013) An overview of protein adsorption on metal oxide coatings for biomedical implants. Surf Coat Technol 233:147–158. https://doi.org/10.1016/j.surfcoat.2013.04.028
4. Wang K, Zhou C, Hong Y, Zhang X (2012) A review of protein adsorption on bioceramics. Interface Focus 2:259. https://doi.org/10.1098/RSFS.2012.0012
5. Das S, Rao KVB (2024) A comprehensive review of biosurfactant production and its uses in the pharmaceutical industry. Arch Microbiol 206:1–27. https://doi.org/10.1007/S00203-023-03786-4
6. Al-Gethami W, Qamar MA, Shariq M, Nasser A, Alaghaz MA, Farhan A, Areshi AA, Hisham Alnasir M (2024) Emerging environmentally friendly bio-based nanocomposites for the efficient removal of dyes and micropollutants from wastewater by adsorption: a comprehensive review. RSC Adv 14:2804–2834. https://doi.org/10.1039/D3RA06501D
7. Wang Z, Furukawa S (2024) Pore-networked soft materials based on metal-organic polyhedra. Acc Chem Res. https://doi.org/10.1021/ACS.ACCOUNTS.3C00655
8. Samin AJ, Taylor CD (2018) First-principles investigation of surface properties and adsorption of oxygen on Ni-22Cr and the role of molybdenum. Corros Sci 134:103–111. https://doi.org/10.1016/J.CORSCI.2018.02.017
9. Yang M, Wang Y, Ma D, Zhu J, Mi H, Zhang Z, Wu B, Zeng L, Chen M, Chen J, Zhang P (2023) Unlocking the interfacial adsorption-intercalation pseudocapacitive storage limit to enabling all-climate, high energy/power density and durable Zn-Ion batteries. Angew Chem 135:e202304400. https://doi.org/10.1002/ANGE.202304400
10. Tao X, Wan J, Liu C, Wang H, Yao H, Zheng G, Seh ZW, Cai Q, Li W, Zhou G, Zu C, Cui Y (2016) Balancing surface adsorption and diffusion of lithium-polysulfides on nonconductive oxides for lithium–sulfur battery design. Nat Commun 7:1–9. https://doi.org/10.1038/ncomms11203
11. Long J, Xi M, Yang P, Huang Z (2024) Mechanisms of metal wettability transition and fabrication of durable superwetting/superhydrophilic metal surfaces. Appl Surf Sci 654:159497. https://doi.org/10.1016/J.APSUSC.2024.159497
12. Cheng J, Cheng X, Wang Z, Jen TC (2024) Enhanced hydrogen storage and CO2 capture capacities on carbon aerogels from Ni-N co-doping. Fuel 372:132271. https://doi.org/10.1016/J.FUEL.2024.132271
13. Huang W, Sun Y, Zhao G, Liu Q, Zhao G, Duan L, An Q, Ren F, Sun M, Xia S, Guo H (2024) Constructing nano spinel phase and Li+ conductive network to enhance the electrochemical stability of ultrahigh-Ni cathode. Mater Today 79:86–96. https://doi.org/10.1016/J.MATTOD.2024.08.002
14. Gao L, Zhan H, Feng G, Ma Y, Zhang C, Zhang Y, Cao M (2024) Engineering mesoporous Na4Mn0.9Ni0.1V(PO4)3@NC microspheres cathode towards advanced sodium ion batteries. J Energy Storage 97:112890. https://doi.org/10.1016/J.EST.2024.112890
15. Zhou L, Li S, Jain A, Chen G, Guo D, Kang J, Zhao Y (2024) Lithium battery thermal management based on lightweight stepped-channel liquid cooling. J Electrochem Energy Convers Storage. https://doi.org/10.1115/1.4063848/1169617
16. Wang C, Chen Y (2024) Unsupervised dynamic prognostics for abnormal degradation of lithium-ion battery. Appl Energy 365:123280. https://doi.org/10.1016/J.APENERGY.2024.123280
17. Inczédy J, Lengyel T, Ure AM et al (1998) Compendium of analytical nomenclature: definitive rules 1997. Blackwell Science, Oxford
18. Siahtiri S, Sahraei AA, Mokarizadeh AH, Baghani M, Bodaghi M, Baniassadi M (2023) Influence of curing agents molecular structures on interfacial characteristics of graphene/epoxy nanocomposites: a molecular dynamics framework. Macromol Mater Eng 308:2300030. https://doi.org/10.1002/MAME.202300030
19. Qi G, Rabczuk T (2019) Ab-initio investigation of lithium adsorption on short carbon nanotubes considering effects of the tube length. Carbon N Y 155:727–733. https://doi.org/10.1016/J.CARBON.2019.08.027
20. Ness C (2023) Simulating dense, rate-independent suspension rheology using LAMMPS. Comput Part Mech 10:2031–2037. https://doi.org/10.1007/S40571-023-00605-X/FIGURES/1
21. Zhong K, Hu R, Xu G, Yang Y, Zhang JM, Huang Z (2019) Adsorption and ultrafast diffusion of lithium in bilayer graphene: Ab initio and kinetic Monte Carlo simulation study. Phys Rev B 99:155403. https://doi.org/10.1103/PHYSREVB.99.155403/FIGURES/11/MEDIUM
22. Vo MD, Shiau B, Harwell JH, Papavassiliou DV (2016) Adsorption of anionic and non-ionic surfactants on carbon nanotubes in water with dissipative particle dynamics simulation. J Chem Phys. https://doi.org/10.1063/1.4949364/913939
23. Reis MC, Alobaid F, Wang Y (2018) Toward the modeling of combustion reactions through discrete element method (DEM) simulations. Comput Part Mech 5:579–591. https://doi.org/10.1007/S40571-018-0191-X/METRICS
24. Demontis P, Pazzona FG, Suffritti GB (2008) Introducing a cellular automaton as an empirical model to study static and dynamic properties of molecules adsorbed in zeolites. J Phys Chem B 112:12444–12452. https://doi.org/10.1021/JP805300Z/ASSET/IMAGES/LARGE/JP-2008-05300Z_0001.JPEG
25. Krzyzanowski M, Svyetlichnyy D (2022) A multiphysics simulation approach to selective laser melting modelling based on cellular automata and lattice Boltzmann methods. Comput Part Mech 9:117–133. https://doi.org/10.1007/S40571-021-00397-Y/FIGURES/17
26. Langmuir I (1918) The adsorption of gases on plane surfaces of glass, mica and platinum. J Am Chem Soc

40:1361–1403. https://doi.org/10.1021/JA02242A004/ASSET/JA02242A004.FP.PNG_V03
27. Pelalak R, Soltani R, Heidari Z, Malekshah RE, Aallaei M, Marjani A, Rezakazemi M, Shirazian S (2021) Synthesis, molecular dynamics simulation and adsorption study of different pollutants on functionalized mesosilica. Sci Rep 11:1–13. https://doi.org/10.1038/s41598-020-80566-w
28. Do DD, Do HD (2006) Modeling of adsorption on nongraphitized carbon surface: GCMC simulation studies and comparison with experimental data. J Phys Chem B 110:17531–17538. https://doi.org/10.1021/JP062386R/ASSET/IMAGES/LARGE/JP062386RF00013.JPEG
29. Knopf DA, Ammann M (2021) Technical note: adsorption and desorption equilibria from statistical thermodynamics and rates from transition state theory, Atmos. Chem Phys 21:15725–15753. https://doi.org/10.5194/ACP-21-15725-2021
30. Hannah F (2008) New statistical mechanical simulation methods for the calculation of surface properties, UCL
31. Fox H, Gillan MJ, Horsfield AP (2009) Methods for calculating the desorption rate of molecules from a surface at non-zero coverage: water on MgO(0 0 1). Surf Sci 603:2171–2178. https://doi.org/10.1016/j.susc.2009.04.015
32. Boghosian BM (1991) Lattice gases illustrate the power of cellular automata in physics. Comput Phys 5:585. https://doi.org/10.1063/1.4823030
33. Pazzona FG, Demontis P, Suffritti GB (2009) From thermodynamic cell models to partitioning cellular automata for diffusion in zeolites. I. Structure of the algorithm. J Chem Phys 131:234703. https://doi.org/10.1063/1.3267635
34. Zhang FF, Huang AQ, Xie SQ, He J (2008) Modeling and simulation of Adsorption and biodegradation in activated sludge process based on cellular automata. Proc IEEE Int Conf Autom Logist ICAL 2008:919–923. https://doi.org/10.1109/ICAL.2008.4636281
35. Chopard B, Masselot A (1999) Cellular automata and lattice Boltzmann methods: a new approach to computational fluid dynamics and particle transport. Futur Gener Comput Syst 16:249–257. https://doi.org/10.1016/S0167-739X(99)00050-3
36. Ziaee O, Zolfaghari N, Baghani M, Baniassadi M (2021) Simulating favorable adsorption in lithium-ion batteries using a novel cellular-automaton-based method. Phys Scr 96:125841. https://doi.org/10.1088/1402-4896/AC2DA4
37. Ziaee O, Zolfaghari N, Baghani M, Baniassadi M, Wang K (2021) A modified cellular automaton model for simulating ion dynamics in a Li-ion battery electrode. Energy Equip Syst. https://www.researchgate.net/publication/355411938_A_modified_cellular_automaton_model_or_simulating_ion_dynamics_in_a_Li-ion_battery_electrode
38. Ziaee O, Zolfaghari N, Baniassadi M, Baghani M (2021) A generalized mobile automaton for simulating particle deposition on a wall: effect of movement rules and wall shape. In: International conference on innovation and research in engineering sciences (ICIRES)
39. Farahvash A, Agrawal M, Peterson AA, Willard AP (2023) Modeling surface vibrations and their role in molecular adsorption: a generalized langevin approach. J Chem Theory Comput 19:6452–6460. https://doi.org/10.1021/ACS.JCTC.3C00473/ASSET/IMAGES/LARGE/CT3C00473_0007.JPEG
40. Luvalle BJ (2019) The effects of boundary conditions on cellular automata. Complex Syst 28:97–124. https://doi.org/10.25088/COMPLEXSYSTEMS.28.1.97
41. Nazzarro M, Nieto F, Ramirez-Pastor AJ (2004) Adsorption thermodynamics of interacting particles on diffusion-limited aggregates. Phys A 331:517–530. https://doi.org/10.1016/J.PHYSA.2003.09.030
42. Vinet L, Zhedanov A, Resnick H (2010) https://www.wiley.com/en-gb/Fundamentals+of+Physics%2C+Extended%2C+10th+Edition-p-9781118547878. Accessed 26 Feb 2023
43. Landau LD, Lifshitz EM (n.d) Statistical physics, 3rd edn, Part 1, vol 5 (Course of Theoretical Physics, vol 5): 9780750633727: Amazon.com: Books. https://www.amazon.com/Statistical-Physics-Third-Part-Theoretical/dp/0750633727/ref=sr_1_1?dib=eyJ2IjoiMSJ9.BvTgmzqTNgTA48Mein0RHnn8LAIXFuSbJWB7kSZkx2wq_nsilYDsFHTty68aeBVt2TvgL1H6pMJ1diKIroIEuk_e2Zdw94jAtxUWQDdMBHsOc2Rf03DkS21hP3jtgXANt1D2U5jhP8ocTdbHTd6Z3CnmDC-yoMY0bnFeuQSfhzocw8UKt1EraLOzkAWgXlJYD173C1CHMU_0LGWKJAoGMU3rIwG2ONqSlqiV48pyVtQG_MZ4a5tPhLjFZIwB0T2wYPCoL-M1bZ3uqGo3N5190g-cAUghrMDpQB35e8WJF8Zeo9EzcllIOflX4uPoWI_3nKGSo3iiZqaMI8agWD5lg6wJyEJNR0sMcTMZW782fm4OBYH1_wASwsSr_MGrkYOFIYv3fJxjV0a03iXuwa-9iUw1aj3z5jLVuwfp2i-I2eB7hO55AF6SE1TJX0OOfrMx.liynWu2jHJ0B3_8UUOe_vOTmk2ewrpwFzhFC5ykbAFQ&dib_tag=se&keywords=Statistical+Physics&qid=1735353595&sr=8-1. Accessed 26 Dec 2024
44. Huang XL, Wang YX, Chou SL, Dou SX, Wang ZM (2021) Materials engineering for adsorption and catalysis in room-temperature Na–S batteries. Energy Environ Sci 14:3757–3795. https://doi.org/10.1039/D1EE01349A
45. Evers S, Yim T, Nazar LF (2012) Understanding the nature of absorption/adsorption in nanoporous polysulfide sorbents for the Li-S battery. J Phys Chem C 116:19653–19658. https://doi.org/10.1021/JP304380J/SUPPL_FILE/JP304380J_SI_001.PDF
46. El-Deen SS, Hashem AM, Abdel Ghany AE, Indris S, Ehrenberg H, Mauger A, Julien CM (2018) Anatase TiO_2 nanoparticles for lithium-ion batteries. Ionics (Kiel) 24:2925–2934. https://doi.org/10.1007/S11581-017-2425-Y/TABLES/1
47. Berendsen HJC, Postma JPM, Van Gunsteren WF, Dinola A, Haak JR (1984) Molecular dynamics with coupling to an external bath. J Chem Phys 81:3684–3690. https://doi.org/10.1063/1.448118
48. Nosé S (1984) A unified formulation of the constant temperature molecular dynamics methods. J Chem Phys 81:511–519. https://doi.org/10.1063/1.447334
49. Matsui M, Akaogi M (1991) Molecular dynamics simulation of the structural and physical properties of the four polymorphs of TiO_2. Mol Simul 6:239–244. https://doi.org/10.1080/08927029108022432
50. Kerisit S, Rosso KM, Yang Z, Liu J (2009) Dynamics of coupled lithium/electron diffusion in TiO_2 polymorphs. J Phys Chem C 113:20998–21007. https://doi.org/10.1021/JP9064517/ASSET/IMAGES/LARGE/JP-2009-064517_0005.JPEG
51. Zeydabadi-Nejad I, Zolfaghari N, Mousavi Mashhadi M, Baghani M, Baniassadi M (2021) Anatase TiO_2 nanotubes as Li-ion battery anodes: a molecular dynamics study of Li-ion Adsorption on anatase nanotubes. Sustain Energy Technol Assess 47:101438. https://doi.org/10.1016/J.SETA.2021.101438
52. Li X, Chao Y, Chen L, Chen W, Luo J, Wang C, Wu P, Li H, Zhu W (2020) Taming wettability of lithium ion sieve via different TiO_2 precursors for effective Li recovery from aqueous lithium resources. Chem Eng J 392:123731. https://doi.org/10.1016/J.CEJ.2019.123731

Publisher's Note Springer Nature remains neutral with regard to jurisdictional claims in published maps and institutional affiliations.